Construction and Building Materials 414 (2024) 135004

Contents lists available at ScienceDirect

Construction and Building Materials

journal homepage: www.elsevier.com/locate/conbuildmat

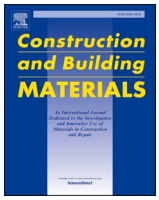

Investigations on the seepage characteristics of polymer grouting body for repairing HDPE geomembrane defects based on LF NMR

Qiuju Ke [a,b], Chengchao Guo [a,b,*], Fuming Wang [a,b], Xuanxuan Chu [c], Kejie Zhai [d]

[a] School of Civil Engineering, Sun Yat-sen University, Guangzhou 510275, China
[b] Southern Institute of Infrastructure Testing and Rehabilitation Technology, Huizhou, China
[c] School of Ocean Engineering, Harbin Institute of Technology, Weihai 264209, China
[d] School of Water Conservancy and Transportation, Zhengzhou University, Zhengzhou 450001, China

ARTICLE INFO

Keywords:
Polymer
Geomembrane
Polymer grouting body
LF NMR

ABSTRACT

As high-density polyethylene (HDPE) geomembranes in landfill liner systems increasingly age and damage, seepage incidents frequently occur and severely threaten the surrounding ecological environment and groundwater safety. Targeted injection grouting with polymer materials can rapidly restore the barrier function by repairing defects in damaged geomembranes. To investigate the sealing mechanisms of polymer grouting bodies with various densities, this study used low-field nuclear magnetic resonance (LF NMR) techniques to monitor and visualize the permeation process within the grouting bodies. The results revealed two failure modes of the grouting bodies under water flows: 1) insufficient interfacial shear strength between the low-density polymer and geomembrane, leading to interfacial leakage; 2) gradual buildup of permeation pressure puncturing the foam cells of the polymer matrix and inducing permeation channels. Selecting polymers with suitable expansion ratios to produce appropriate expansive pressures is crucial to enhance interfacial shear strength while avoiding secondary damages to geomembranes. Increasing the density of the polymer grouting body can also enhance the compressive strength of foam cells and interfacial shear resistance. These are crucial for enabling grouting repair of defects in geomembranes and improving their barrier performance.

1. Introduction

Leachate exfiltration, runoff and slope failure are common issues at landfills during operation. They can severely impact the environment and society. Leachate exfiltration is particularly prominent, and thus the landfill liner system is a critical component that can directly affect normal landfill operation. High-density polyethylene (HDPE) geomembranes have been widely adopted at modern landfills as impermeable barriers [1,2]. Global studies indicate that improper mechanical processing or human errors may induce geomembrane defects during installation of artificial liners, causing potential seepage pathways along seams. During landfill operation, non-uniform settlement of the subgrade, excessive height of waste piles, mechanical damages and chemical degradation may also lead to geomembrane leakage [3–5]. It is evident that geomembrane failure is one major contributor to landfill leakage [6,7]. Once these defects are not identified and repaired in time, leachate can migrate into groundwater and soil, imposing long-term and severe subsurface contamination. Therefore, research and development of HDPE geomembrane defect restoration technologies is of significant practical value for landfills.

Geomembrane defects induced during installation of landfill liners and construction of overlying drainage layers and leachate collection facilities can be easily repaired. However, repair conditions during operation and closure periods are complex (typically requiring a water-free or waste-free environment). Conventional repair procedures involve extensive excavation and dewatering to expose leakage locations, which are laborious, time-consuming. These procedures can disturb normal landfill operation and cause secondary contamination over large areas. Therefore, economical, efficient and safe repair techniques are urgently needed for remediation of defects in landfill impermeable barriers.

With the development and application of novel materials, chemical grouting technologies represented by non-water reacting polymers have garnered extensive attention worldwide for their rapid leak-plugging efficacy [8]. Targeted grouting repair techniques with polymer materials have been extensively applied for remediation and reinforcement of

* Corresponding author at: School of Civil Engineering, Sun Yat-sen University, Guangzhou 510275, China.
E-mail address: guochch25@mail.sysu.edu.cn (C. Guo).

https://doi.org/10.1016/j.conbuildmat.2024.135004
Received 25 October 2023; Received in revised form 19 December 2023; Accepted 10 January 2024
Available online 20 January 2024

damages in foundational infrastructure facilities, including dams, tunnels, underground corridors, highways and airfield runways. Fig. 1 shows engineering case studies of using targeted polymer grouting for seepage blocking in China. The fundamental principle of this technique is the use of targeted grouting equipment to inject instant mixtures of two-component polymer materials towards identified seepage or defect areas. The injected grout rapidly expands in volume upon mixing and solidifies to form a foam "plug" of certain strength, achieving rapid void filling, seepage prevention, leakage blocking and surrounding rock consolidation [9–12]. Targeted grouting techniques enable precise repair of damaged areas with high material utilization. Compared to traditional grouting materials, polymer materials possess superior flowability and penetrability, allowing accurate repair of target locations.

Currently, extensive studies have been conducted on the grout diffusion laws and reinforcement performance of polymers in underground environments. Li et al. [13] used an unsplit Youngs method to track the moving interface of expansible polymer grouting fractures. Compared with the analytical solution and the traditional split Youngs algorithm, the unsplit Youngs method significantly improved the accuracy of tracking the moving interface. Wang et al. [14] established the random field model of reinforcement and analyzed the influence of permeation polymer curtain grouting reinforcement measures on failure probability of different types of slopes. Guo et al. [15] investigated the diffusion behavior of an expanding polymer grouting material in sand, gravel and a sand-gravel mixture through in situ grouting tests. It is found that the diffusion depends mainly on the size of pores and particles of the medium, with polymers spreading predominantly by permeation in loose media and advection in fine-grained media. Wang et al. [16] adopted full-scale field testing under combined ground impact and driving loads to examine the structural dynamic responses of a reinforced concrete drainage pipe buried in dense soil before and after non-excavation polymer grout repair. The results showed that polymer grouting can effectively repair detached pipes and even restore the mechanical performance to the level of intact pipes. Hao et al. [17] utilized a self-designed visible fracture grouting device to study the diffusion behavior of polyurethane grouts in water-filled fractures under various conditions. The effects of grouting amount and water pressure on the grout diffusion distance and flow fields were revealed. Du et al. [18] performed permeability and uniaxial compression tests on grouted specimens to examine the anti-seepage reinforcement effects of permeative polymer grouting on drainage pipes in loose zones in terms of factors including water head pressure, grouting pressure, sand particle size and clay content. Zhou et al. [19] performed various laboratory tests to study the effects of grouting temperature, water-binder ratio and mass fractal dimension on the viscosity, pore occupancy in the injection medium and pressure changes under constant conditions. Sun et al. [20] investigated the grouting reinforcement effects of a new soluble foamed polymer grout on fragmented coal bodies compared to conventional ultrafine cement and aluminate cement grouts. They found that the new polymer material can effectively bond cracks and fractures in raw coal and significantly improve concrete strength.

The mechanism of polymer grouting has been extensively studied in underground environments. However, due to the concealed nature and large-scale of grouting reinforcement and anti-seepage projects, as well as the complex geological conditions of landfills, it is difficult to obtain in-situ samples of the grouting body. Therefore, traditional testing methods and in-situ construction cannot observe the conditions before

Fig. 1. Application cases of polyurethane grouting materials in China for seepage prevention: (a) a dam; (b) a landfill dam; (c) a shield tunnel; (d) a levee.

and after grouting repair. Additionally, the grouting leak-blocking theory spans multiple disciplines, including materials science, chemistry, and fluid mechanics. Currently, the grouting theory still lags behind engineering practice and lacks scientific and reasonable technical guidance. As a "plugging body", the polymer acts upon to block seepage channels. However, under high hydraulic pressure, shear forces are developed between the polymer "plugging body" and the surrounding soil. When these shear forces exceed a certain threshold, interface failure and shear displacement can occur, which can potentially displace the polymer and cause plug failure. Therefore, it is necessary to study the seepage characteristics of polymer grouting body to explore the interaction between water, polymers, and geomembranes. This will help reveal the mechanism of polymer grouting in sealing leakage in landfill anti-seepage layers, which is crucial for effectively preventing embolism failure and assessing the application prospects of this new technology and improving engineering practice. Conventional tests can hardly observe the rheological processes inside the grouting body directly. Nuclear magnetic resonance (NMR) technology has the advantages of non-destructive, rapid and safe detection and monitoring and has been widely used in the fields of (e.g.) life sciences, energy geology, agriculture, food and aerospace [21–25]. This study employed low-field NMR (LF NMR) techniques to conduct infiltration tracer tests and imaging on grouting bodies with different densities. Then, the failure mechanism, interaction mechanisms and coupling effects of polymer "plugging bodies" under seepage conditions were further revealed. The findings can clarify the failure patterns of grouting bodies under seepage conditions, providing a theoretical basis for optimizing the parameters of polymer grouting materials. This can contribute to designing reasonable seepage control and leakage repair solutions based on different site conditions and scales of damage, thereby improving the long-term stability of landfills.

2. Test design

2.1. Specimen preparation of polymer grouting body

The non-water two-component foamed polyurethane grouting material, produced by Yantai Wanhua Polyurethane Co, Ltd, was used to repair high-density polyethylene (HDPE) geomembrane with an 8 mm diameter circular hole, simulating the defect scenario. First, HDPE geomembrane cylinders (50 mm in diameter, 50 mm in height, 2 mm in thickness) were fabricated by injection molding. A circular hole with 8 mm diameter was prepared at the center of the bottom of the geomembrane to simulate geomembrane damage. Artificial municipal solid waste (MSW) was formulated with the composition in Table 1, with a dry density of 0.63 g/cm^3 and a porosity of 0.7. Clayey soil was placed under the geomembrane to simulate the subgrade soil of landfill sites, with physical properties listed in Table 2. In order to ensure comparability of the grouting specimens, the physical properties of all specimens for both artifical MSW and clayey soil remains consistent. Then, a rubber membrane was wrapped on the inner surface of the grouting mold, followed by layered addition of clayey soil, geomembrane with hole and simulated MSW from bottom to top. The grouting pipe with a diameter of 3 mm was pre-embedded to the bottom of the clayey soil. After filling and compacting each layer of soil, use a fine round stick to further compact it. When filling the next layer of soil, roughen the surface of the already compacted soil layer to ensure intimate contact between the upper and lower layers. Finally, a Graco Inc's precise grout injection device, EFR-2ADDC, was used to inject the polymer grout slurry at a preset mass ratio into the mold. Then quickly pulled out the grouting pipe and tightly sealed the mold top. The slurry diffused upwards along the vertical fissures until reaching the geomembrane defects and penetrating into artificial MSW, forming an isolation body. The specimens were demolded after curing for 20 min. Cylindrical grouting specimens were prepared with a diameter of 50 mm and a height of 90 mm. The grouting equipment and the internal structure of the grouting body are shown in Fig. 2.

Table 2
Physical properties of clayey soil.

Natural density (g/cm^3)	Natural water content (%)	Liquid limit (%)	Plastic limit (%)
2.012	19.1	38.89	20.33

2.2. Test scheme and procedure

2.2.1. Test apparatus

An LF NMR monitoring system (MacroMR12–110 H-GS-HTHP, Suzhou Niumag, China) was utilized to conduct the grouting body flooding tests. The apparatus consisted of a NMR core analysis system, non-metallic core holder, liquid and gas injection system, high and low temperature and high-pressure circulation system and data acquisition system, as illustrated in Fig. 3. Specifically, the NMR module was a MacroMR12 system with a radio frequency pulse frequency range of 1–30 MHz and a maximum sampling bandwidth of 2000 kHz. The magnet had a magnetic field intensity of 0.52 T. The primary material of the core holder was polyether ether ketone (PEEK) resin fabricated in a large size (capable of containing samples with a diameter of 50 mm and a length of 100 mm) without NMR signals. Various confining pressures were achieved by injecting fluorocarbon oil, with the maximum confining pressure up to 5 MPa. The driving force for the test permeation was provided by a dual-cylinder constant pressure/constant flow displacement pump with pressure range of 0–40 MPa and flow rate range of 0–50 mL/min.

2.2.2. Test scheme

Considering that the grouting volume is a critical factor affecting the plugging efficiency of the grouting body, this study selected different grouting mass and conducted four groups of tests. The specific schemes of which are shown in Table 3.

2.2.3. Test steps

The water flooding test on the grouting body was conducted at a constant flow rate (see Fig. 4). Firstly, the specimens were placed in low-temperature oven at 30 ℃ until their weights stabilized to remove moisture. Then, the specimens were installed in the clamp and connected to the test device. The displacement device was linked and flushed with water while venting air. However, a confining pressure was needed to prevent surface flow of the specimen. Excess confining pressure could lead to severe deformation, resulting in cracks at the interface between the geomembrane and the polymer and eventually failure. Through preliminary tests, it was determined that applying an initial confining pressure of 1 MPa and maintaining a pressure differential of 1 MPa between the confining pressure and displacement pressure during flooding could both prevent surface loss and avoid excessive deformation. Initially, an initial confining pressure of 1 MPa was applied, followed by injecting water at a constant flow rate of 0.1 mL/min for about 1 h until the inlet pressure reached 0.01–0.02 MPa. Subsequently, the NMR technology was used to characterize the one-dimensional and two-

Table 1
Composition of artifical MSW.

Component	Bran	Paper	Wood	Fiber textile (Rags)	Plastic rubber	Granules	Mixed soil
Proportion (wt%)	40	15	10	5	10	10	10

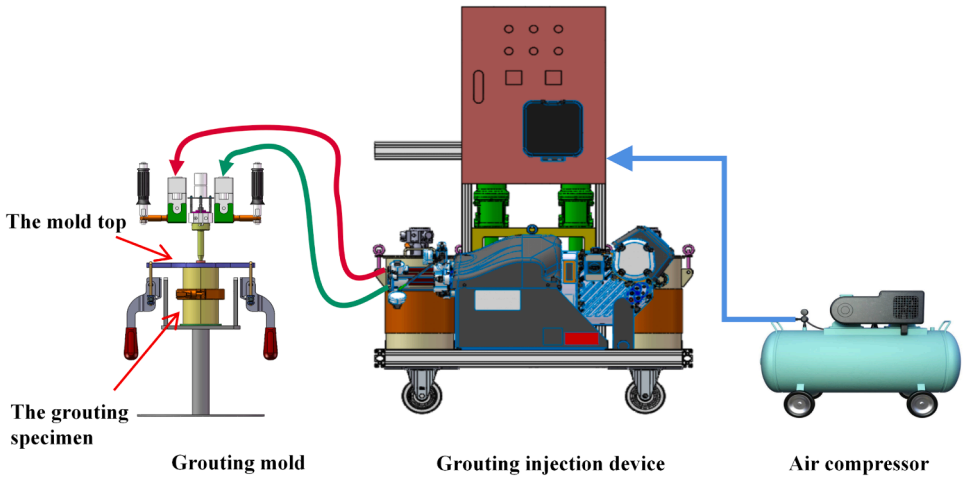

(a)

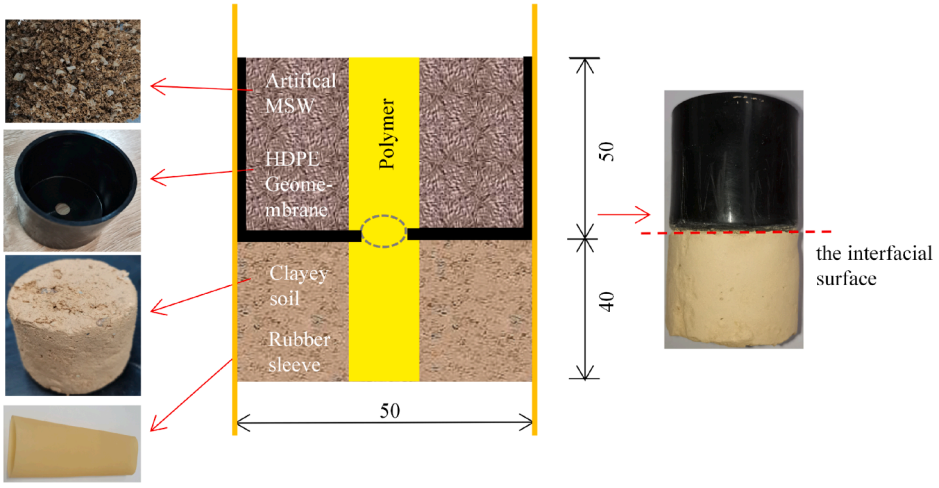

(b)

Fig. 2. Schematic diagram of grouting device and the internal structure of grouting body: (a) grouting device; and (b) grouting body.

dimensional spatial distribution of water in the specimen to obtain its initial structural features. After injecting at a steady flow rate of 0.1 mL/min for a period, the NMR technology was utilized again to depict the spatial distribution of water in the specimen to acquire the structural characteristics at that moment. The previous step was repeated to monitor the structural data of the specimen at different times until leakage of the grouting body occurred. Finally, the specimen was dismantled. The density of the polymer in the grouting body and moisture content of clayey soil was tested. Scanning electron microscopy was used to observe the microscopic morphology of the polymer at the interface in the grouting body.

3. Results

3.1. Macroscopic morphology and microscopic topography of polymers in grouting body

After the flooding test, the specimen was dismantled. The geomembrane and clayey soil in the grouting solution showed no obvious deformation. Although Fig. 7 shows noticeable deformation of the sample cross-section during the seepage process because the pressure difference between the confining pressure and inlet pressure was maintained at 1 MPa, most of the deformation could be recovered after removing the confining and flooding pressures on the sample. This indicates the deformation occurred in the seepage test was within an acceptable range.

3.1.1. Macroscopic morphology of polymer

The macroscopic morphology of the polymer in the grouting body with different grouting mass is shown in Fig. 5. Due to the irregular shape of the polymer in the grouting body, its volume was measured by the drainage method and weighed using a balance, in order to obtain the density of the grouting body and moisture content of the clayey soil in the grouting body (Table 4). The polymer slurry was first injected into the clayey soil at the bottom of the mold. As vertical fissures rapidly propagated upwards, it penetrated through the damaged geomembrane into artificial MSW with larger porosity, forming a relatively uniform "barrier" from bottom to top. Fig. 5 shows that the diffusion forms of the polymer differed in different media. After filling the fissures in the clayey soil, with increasing expansive force, the polymer solution split the soil body randomly in uneven lengths. In artificial MSW with larger porosity, the polymer mainly permeated and cemented, closely bonding

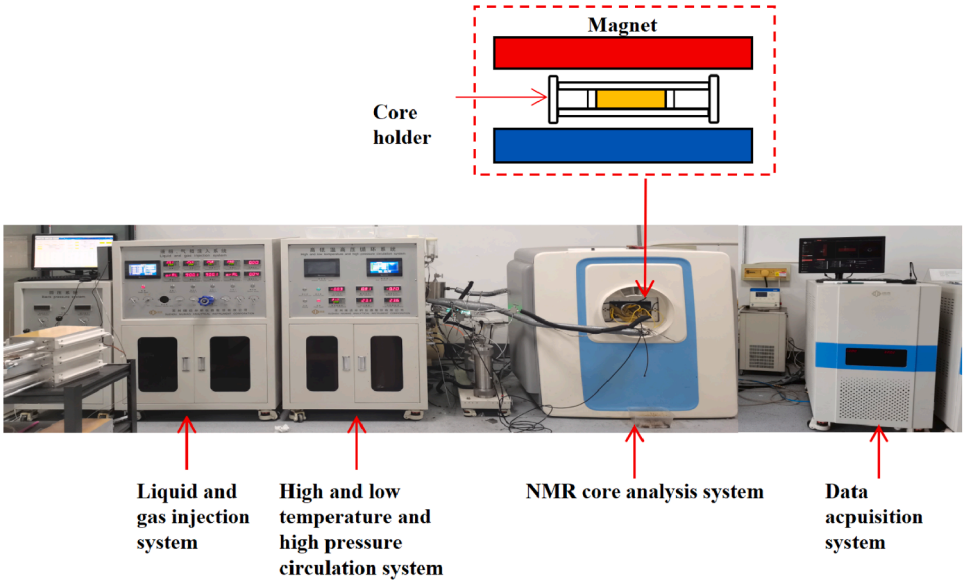

Fig. 3. Schematic diagram of the online nuclear magnetic resonance analysis system.

Table 3
Test scheme design for grouting body specimens.

Sample No.	Grouting mass /g	Leakage hole diameter in geomembrane /mm
1	7	8
2	10	8
3	15	8
4	20	8

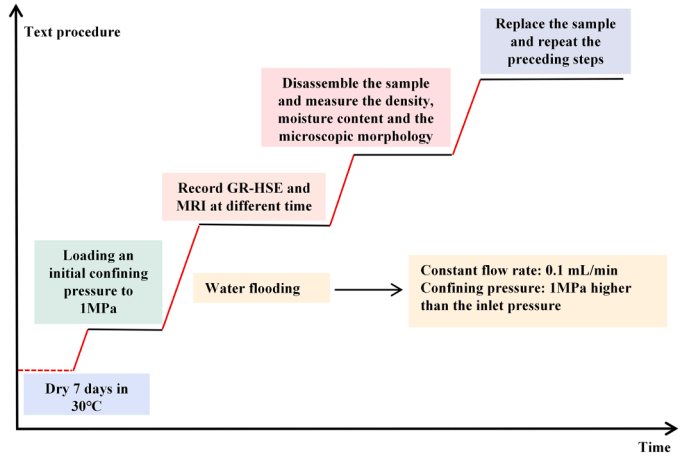

Fig. 4. Text procedure of the water flooding.

with materials such as plastics, cloth and paper in artificial MSW. As the grouting mass increased, the volume of the solidified polymer increased, and the slurry at the contact interface between the polymer, geomembrane and clayey soil gradually accumulated. As shown in Fig. 5(b), (c) and (d), a polymer layer formed at the interface, tightly bonding with the geomembrane. This layer can play a repairing role and provide additional seepage-proofing, enhancing the anti-seepage performance of the structure.

3.1.2. *Microscopic morphology of polymer at the interface*

The microscopic morphology of the polymer at the polymer-clayey soil interface is shown in Fig. 6. The polymer grouting material consisted of densely arranged closed foam cells. The foam cells were circular, polygonal or elliptical in shape, and the cells were not interconnected. As the grouting mass increased, the polymer density was gradually elevated, and the diameter of the foam cells was reduced. At lower densities, the diameter of the foam cells was larger; the gas content was higher; the cell walls were thinner. At higher densities, the diameter of the foam cells was smaller; the gas content was lower; the cell walls were thicker.

The sample with the smallest grouting mass (Fig. 6(a)) showed no significant water flow impacts on the foam cells, indicating that water flowed around the polymer. Table 4 shows that after the flooding test, the clayey soil in the sample absorbed more moisture, with the water content reaching 12.6%. This suggests that under the effect of water flow, the interface between the geomembrane and the polymer was breached, and water leaked mainly from the interface. Meanwhile, in the three samples with higher densities in Fig. 6(b), (c) and (d), some pores existed in the polymer being ruptured by the impact of the water flow. The water content in the clayey soil was below 4% in all cases. This indicates that under a high water pressure, the water flow ruptured some of the polymer pores, forming preferential pathways for water to leak from the polymer.

3.2. *One-dimensional and two-dimensional dynamic distribution of fluid in the grouting body during flooding*

To study the distribution law of fluid in grouting bodies with different grouting mass during flooding, the NMR imaging technology was used to dynamically monitor the seepage and spatial distribution of fluid in the grouting body. The signal intensity of the NMR image reflected the filling condition of fluid in pores at different parts of the grouting body sample. A low MRI signal intensity (blue area) corresponded to low water content, whereas a high MRI signal intensity (red area) corresponded to high water content[26]. By analyzing the signal intensity distribution in images of different samples, the filling and distribution characteristics of fluid in the internal space of each sample can be determined.

Figs. 7 and 8 show the NMR images and one-dimensional water distribution graphs of the sample with grouting mass of 7 g at different stages during the flooding process. In the stage within the first 15 min, it was mainly the self-absorption of water by artificial MSW, and the water content in artificial MSW gradually increased. There was a clear boundary between the polymer region and artificial MSW region, and almost no water existed in the polymer region. When artifical MSW

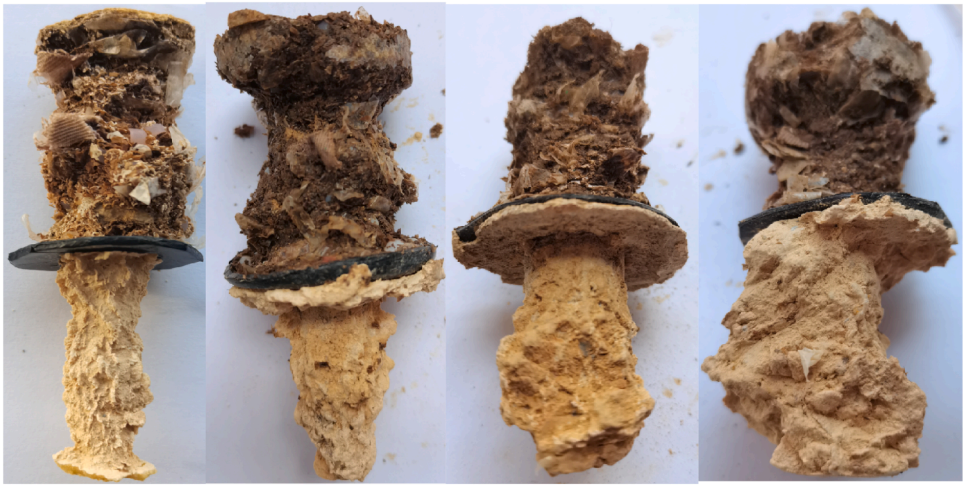

(a) (b) (c) (d)

Fig. 5. Macroscopic morphology of polymer in the grouting body with different grouting mass: (a) 7 g, (b) 10 g, (c) 15 g and (d) 20 g.

Table 4
Parameters of the grouting body.

Sample No.	Grouting mass (g)	Density (g/cm^3)	Moisture content of clayey soil (%)
1	7	0.23	12.6
2	10	0.33	3.9
3	15	0.44	2.3
4	20	0.56	3.5

reached a saturated state, the fluid began to accumulate at the interface between the polymer and the geomembrane. The fluid volume continued to increase. After being displaced to 30 min, with the increase of inlet pressure and confining pressure, the sample underwent slight deformation. A weak fluid signal occurred in the clayey soil area on the right side of the interface. At the same time, an obvious fluid signal also occurred in the permeable rock zone on the right side. The above results indicate that leakage occurred in the grouting body. In conjunction with Fig. 6(a), no apparent hydraulic fracturing was observed in the polymer foam cells at the interface, and the water content of the clayey soil was relatively high after the water flooding test. It can be inferred that for this specimen, water flowed around the polymer region and leaked through the interface between the polymer and geomembrane.

During the water flooding process, the fluid distribution characteristics at different times and spatial locations of the three groups of grouting body samples with 10 g, 15 g and 20 g grouting masses were relatively similar. The sample with 15 g grouting mass was taken as an example. Fig. 9 shows the NMR imaging results of this sample at different times during the water flooding process. Fig. 10 measured the fluid distribution at different positions of the grouting body during water flooding using the one-dimensional frequency encoding technique. Figs. 9 and 10 show that in the first 15 min, it was mainly the self-absorption of water by artificial MSW, and the water content in artificial MSW gradually increased. There was a clear boundary between the

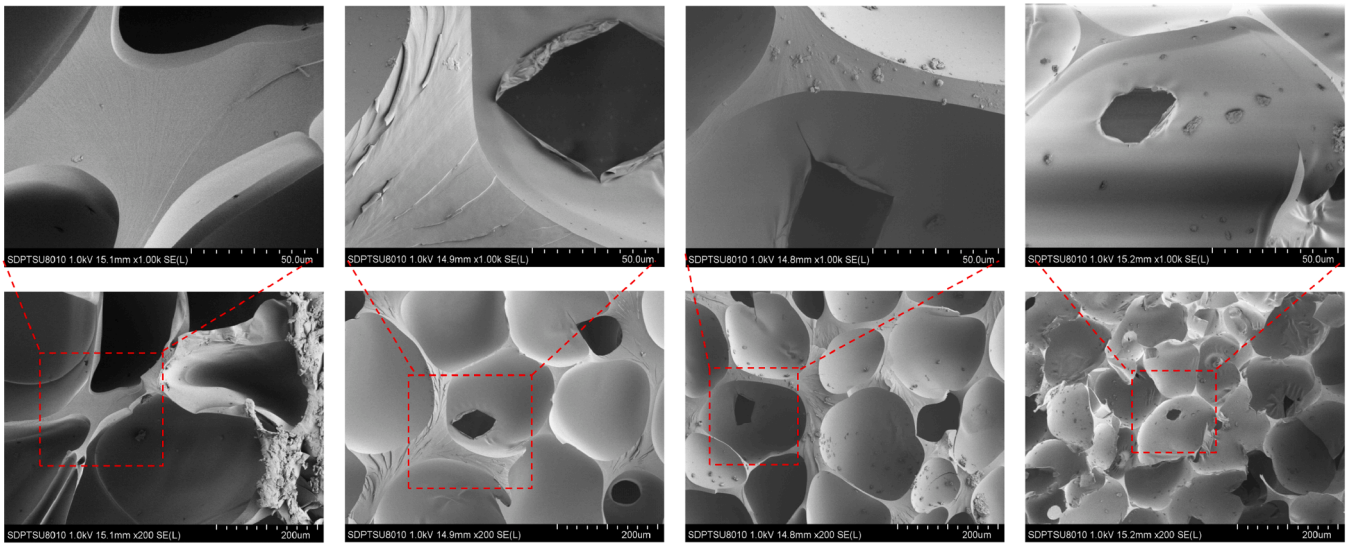

(a) (b) (c) (d)

Fig. 6. Microscopic morphology of polymer at the interface in grouting body with different grouting mass: (a) 7 g, (b) 10 g, (c) 15 g and (d) 20 g.

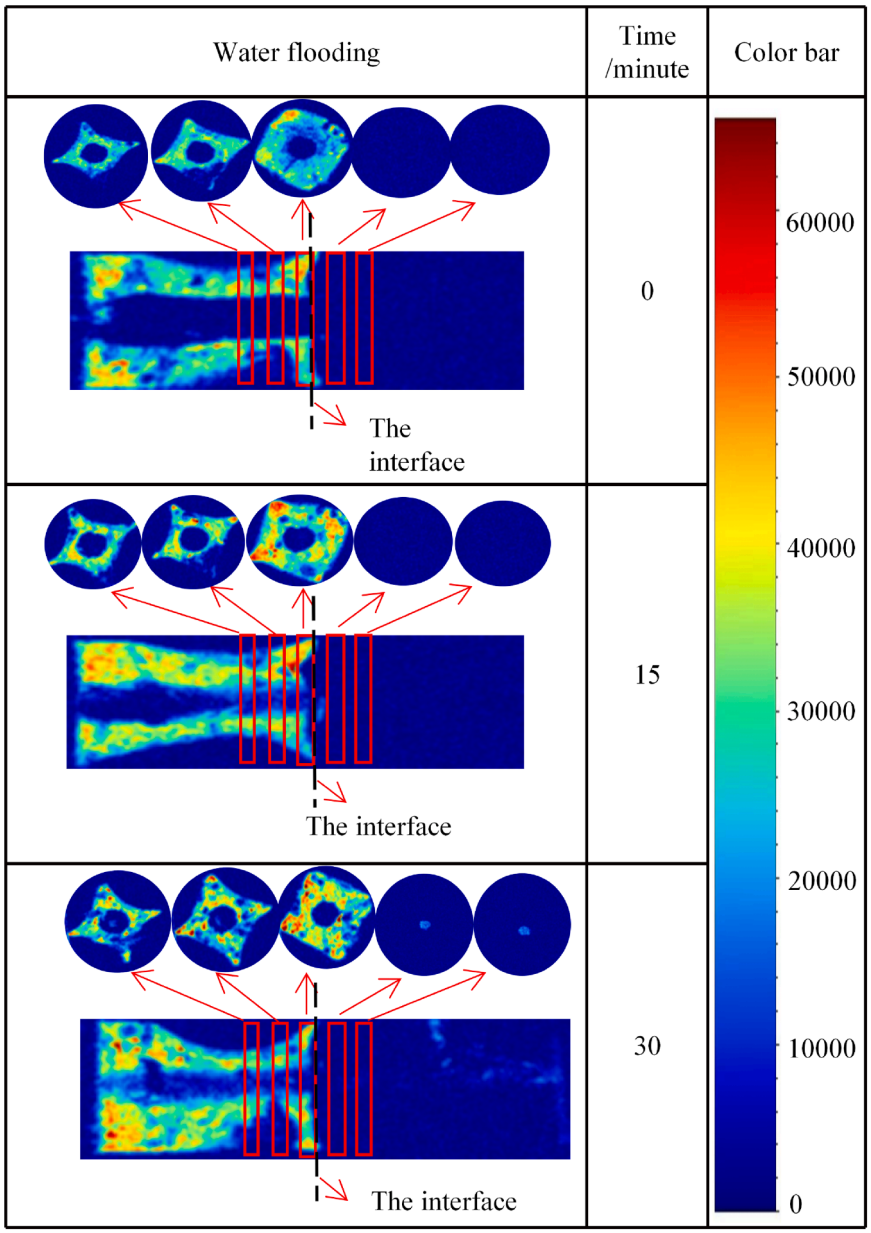

Fig. 7. MRI in the grouting body with a grouting mass of 7 g.

polymer region and artificial MSW region, and almost no water existed in the polymer region. When displaced to 30 min, a small number of water signals appeared in the polymer region. This indicates that with the increase of pressure, the water flow broke through the polymer skin structure and water began to enter the polymer foam cells. As the pressure increased, the surface layer of the polymer was breached, and water began to enter the polymer foam cells. When displaced to 40 min, the water signal in the polymer continued to increase, and water kept filling the foam cells. When displaced to 50 min, the water flow broke through the interface between the geomembrane and the clayey soil. Significant water flow signals were detected at the right end of the interface, indicating that leakage of the grouting body occurred. Fig. 6 (c) shows that obvious penetrative traces existed in some of the polymer foam cells at the interface. Meanwhile, the clayey soil had a relatively low water content after the flooding test. It can be inferred that during the flooding process, the water flow impacted and damaged the polymer foam structure, resulting in interconnected leakage channels and internal leakage within the polymer matrix.

3.3. Inlet pressure analysis

Fig. 11 shows the change of inlet pressure σ_1 with time during the water flooding process for grouting bodies with different grouting masses. For the sample with a relative small grouting mass in Fig. 11 (a) (with a polymer density of 0.23 g/cm^3), its inlet pressure increased almost linearly with the prolongation of displacement time until reaching the peak value of 0.35 MPa and then began to decrease. This indicates that in the initial stage of displacement, sufficient water absorption and volume expansion occurred in the artifical MSW. When the artifical MSW approached saturation, seepage water began to accumulate at the bottom of the geomembrane, forming local pore pressure. Under the continuously increasing pressure, contact damage occurred at the interface between the geomembrane and polymer, resulting in interface seepage. Then, the pore pressure was released, reducing the inlet pressure.

For the samples with larger grouting mass in Fig. 11 (b), (c) and (d) (with polymer densities of 0.33, 0.44 and 0.56 g/cm^3, respectively), sufficient water absorption occurred in the artifical MSW layer, and the

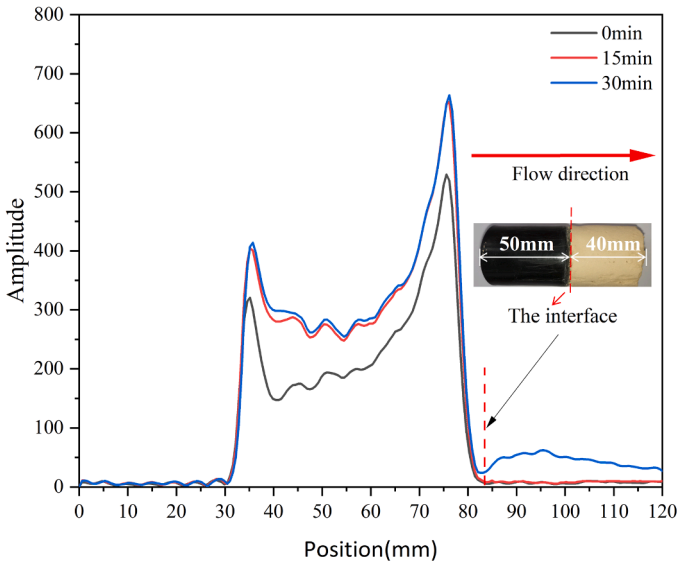

Fig. 8. One-dimensional water distribution of the grouting body with a grouting mass of 7 g.

inlet pressure slowly increased. As the pressure continued to increase beyond the impermeability threshold of the polymer, the water flow broke through the polymer surface layer and penetrated inward. The increasing rate of inlet pressure accelerated until reaching the peak value. Subsequently, water flow signals were detected on the right side of the interface. Finally, water completely breached the polymer and formed dominant seepage channels, reducing the inlet pressure.

By monitoring the changes in the inlet pressure and comparing with the NMR images, the leakage period of the grouting body during the flooding process can be clearly determined. Therefore, the maximum inlet pressure before leakage during the flooding process can be adopted as an important indicator to evaluate and characterize the anti-seepage performance of the grouting body. This pressure was defined as the seepage initiation pressure. With the increase of grouting mass, the seepage initiation pressure of the grouting body showed an increasing trend, indicating enhanced anti-seepage performance. However, the influence of different leakage mechanisms on the seepage initiation pressure needs to be noted. When seepage occurred along the interface between the polymer and geomembrane, the corresponding seepage initiation pressure was significantly lower than that caused by internal damage and penetration of the polymer. The analysis of test results shows that the seepage initiation pressure was about 0.35 MPa for interface leakage. For internal damage leakage of the polymer, the seepage initiation pressure was higher, exceeding 2 MPa. This significant difference can be attributed to the lower interfacial shear strength when the polymer density was low, which easily caused interface damage and leakage under lower pressure. In comparison, the interior of the polymer was a discontinuous closed-pore structure that required sufficient water pressure to break through its internal structure and generate seepage channels.

4. Discussion

4.1. Analysis of the failure modes of the grouting body under water flow

Under the fluid action, two primary leakage failure mechanisms of the grouting material were identified. The first mechanism was that the fluid induced hydraulic fracturing at the interface between the polymer and geomembrane, causing shear failure and leakage along the interface. This is because the shear stress at the interface exceeded the interfacial shear strength. The second mechanism was that the fluid punctured through the weaker sections inside the foam structure of the polymer, forming preferential seepage channels within the polymer matrix. The water mainly leaked through the interconnected pores and channels inside the polymer. The two failure mechanisms are analyzed as follows.

4.1.1. Interface seepage mechanism

When the geomembrane had larger defects or the grouting mass was smaller, the density of the polymer was lower. The expansive force generated by the grout-medium reaction was weaker, resulting in a weaker plugging force at the polymer-geomembrane interface. Owing to the polymer's inherent good anti-seepage performance, higher water pressure was required to erode its surface structure and damage the internal foam pore structure. When the water pressure was insufficient to damage the polymer surface layer, water flow first caused leakage at the polymer-geomembrane interface. In such cases, the seepage initiation pressure of the grouting body was usually lower. The anti-seepage performance of the grouting body mainly depended on the interfacial shear strength between the polymer and geomembrane. This shear strength was influenced by multiple factors, primarily derived from the frictional resistance of the polymer and geomembrane themselves. The expansion pressure generated by the expansion of the polymer grout at the cross section of geomembrane defects. Leakage and damage occurred when the interfacial shear strength was inadequate.

Based on seepage shear stress theory, the interface seepage mechanism of the grouting body under constant water flow mainly went through the following three stages:

5. Initial stage

Under constant velocity water flow, water is first adsorbed by the artificial MSW particles in the grouting body. When the artificial MSW reaches a saturated state, the fluid accumulates at the interface between the polymer and geomembrane, gradually forming an initial infiltration pressure. At this stage, the shear stress generated on the interface is lower than the interfacial shear strength, and the interface remains intact.

(1) Pressure accumulation stage: After the initial stage, the amount of fluid at the polymer-geomembrane interface continues to increase, and the corresponding inlet pressure also increases with time. In this stage, the inlet pressure at the interface causes a shear stress. However, this pressure is still lower than interfacial shear strength, and the interface is not damaged.
(2) Failure stage:
(3) As the pressure accumulation stage progresses, the infiltration pressure at the polymer-geomembrane interface keeps increasing. When it rises to a critical value, the corresponding interfacial shear stress (denoted as τ_1) also reaches the critical value of the interfacial shear strength (denoted as τ_{sc}), i.e., $\tau_1 = \tau_{sc}$. According to the Coulomb fracture criterion, when the applied shear stress reaches the material shear strength, material failure and yielding will occur. Therefore, when $\tau_1 \geq \tau_{sc}$, yielding and fracture occur at the geomembrane interface. Seepage penetrates the interface to form through seepage, with the seepage flow rate showing an increasing trend. This marks the occurrence of the destruction stage of seepage failure.

The interfacial shear stress is mainly generated by the momentum exchange caused by the velocity change of water molecules passing through tiny pores during seepage. The shear stress is related to the seepage velocity:

$$\tau_1 = k_1 \rho v A t \tag{1}$$

where τ_1 is the interfacial shear stress, $\rho$is the fluid density, v is the flow velocity, A is the cross-sectional area in contact with the fluid, t is the

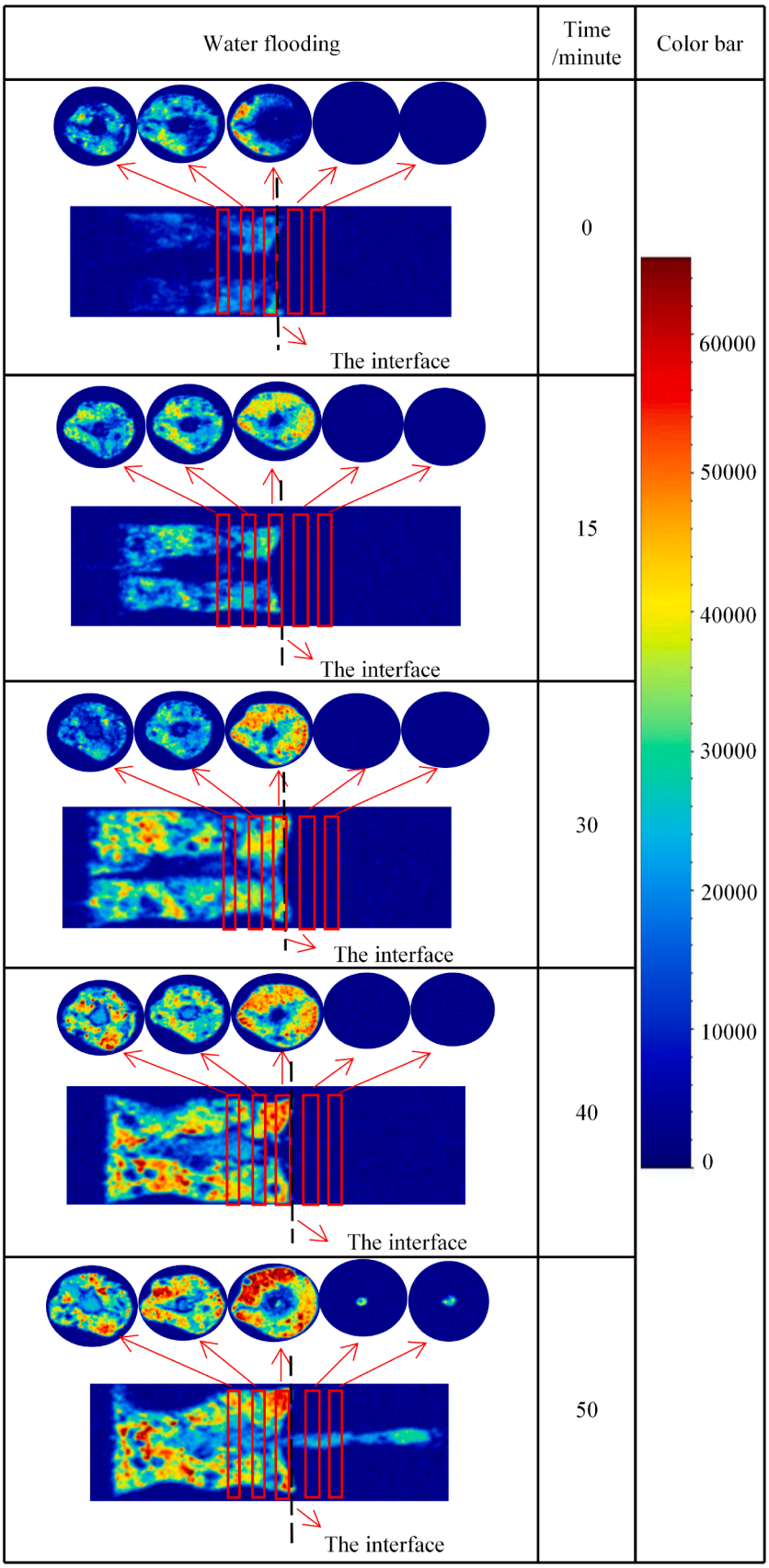

Fig. 9. MRI in the grouting body with a grouting mass of 15 g.

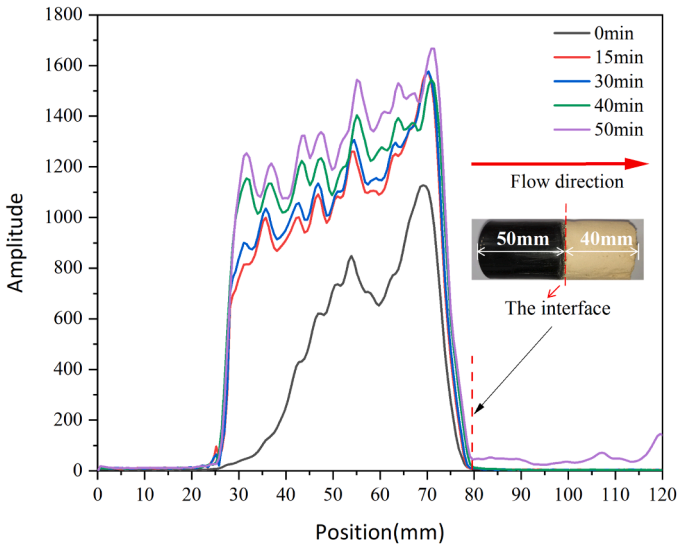

Fig. 10. One-dimensional water distribution of the grouting body with a grouting mass of 15 g.

seepage time and k_1 is an empirical coefficient related to fluid properties and interface morphology.

The interfacial shear strength is composed of two components: frictional shear resistance, generated by the expansion pressure of the polymer swelling effect acting on the cross-section of the geomembrane was determined as

$$\tau_f = \mu P \tag{2}$$

where$\mu$is the interface friction coefficient,$P$is the expansion pressure; and the shear strength between the polymer and geomembrane materials which was expressed as

$$\tau_0 = cA \tag{3}$$

where c is the shear strength coefficient of the material and $A$is the cross-sectional area.

Thus, the interfacial shear strength can be expressed as

$$\tau_{sc} = \mu P + cA \tag{4}$$

Based on the aforementioned analysis, interface failure occurs when the seepage shear stress exceeds the shear resistance of the interface material. The critical condition for interface failure can be characterized by

$$k_1 \rho v A t \geq \mu P + cA \tag{5}$$

Transforming the above equation, the critical uplift pressure when interface failure occurs can be obtained as:

$$P_c = (k_1 \rho v A t - cA)/\mu \tag{6}$$

The analytical expression for the critical uplift pressure at interface failure shows that the threshold value for interface failure is directly proportional to the seepage force while being inversely correlated with the interfacial shear resistance coefficient. The following integrated technical measures should be adopted in order to maximize the safety margin between the critical uplift pressure and the actual uplift pressure, thereby ensuring the long-term stability of the grouting interface:

(i) From the perspective of seepage control, optimize the drainage and collection system of the landfill to monitor; regulate underground water flow; restrain seepage velocity; mitigate the shearing effect on the interface due to momentum transfer; reduce the driving force for interface failure.

(ii) Regarding material design, selecting superabsorbent polymers with appropriate swelling ratios to generate modest swelling pressure can provide the requisite positive stress to reinforce the interface while averting excessive uplift pressure resulting in secondary damage to the geomembrane. Modifying the compositional structure of the superabsorbent polymer to increase the coefficient of friction with the geomembrane can enhance the interfacial shear strength between them.

(iii) In terms of interface structural design, implement meticulously devised grouting arrangements to rationally regulate the dispersion and permeation of the polymer slurry on the geomembrane surface. Thus, a barrier of sufficient thickness can be developed at the interface, which furnishes the necessary positive stress while also performing seepage control, thus improving the overall interfacial shear performance.

5.1. *Internal seepage mechanism of polymer*

With the increase of grouting mass, the density of the polymer increased accordingly. The expansive force of the polymer in the artificial MSW, geomembrane defects and cohesive soil also increased correspondingly. The interfacial shear strength of the grouting body was relatively large, meaning the polymer slurry can “plug” the geomembrane defects well. Water gradually penetrated the polymer foam cells. Thus, the internal seepage mechanism of the polymer comes into play. Under such circumstances, the impermeability of the grouting body depended primarily on the intrinsic impermeability of the polymer.

Under the effect of constant water flow, the internal seepage mechanism of the polymer in the grouting body mainly involves the following three stages:

(1) Loading stage: At high polymer densities, the resultant swelling forces are greater, conferring enhanced shear resistance at the polymer-geomembrane interface. The seepage pressure exerted by the water flow acts upon the interface. However, owing to the high interfacial shear resistance, the seepage cannot immediately rupture the interface. The seepage pressure incrementally compresses the foam cells within the polymer structure.

(2) Initial damage stage: When the seepage pressure surpasses the compressive strength of the fragile foam cells, these cells begin to fail. Some large-diameter thin-walled foam cells will first undergo elastoplastic deformation and damage. The rupture of foam cells leads to imbalance between the internal and external pressures, allowing water molecules to enter the cells. Localized damage then starts to occur in the polymer material. However, the interfacial shear resistance remains high, and thus the water flow is still unable to directly rupture the interface.

(3) Damage propagation stage: The number of ruptured foam cells from the initial damage gradually increases, with more adjacent fragile foam cells also bursting under the water pressure. The various damaged regions expand and progressively coalesce, enlarging the scope of damage, eventually forming seepage channels that penetrate through the polymer material. Concurrently, when the water pressure surpasses the interfacial shear resistance, interface failure and rupture occurs. Meanwhile, internal seepage within the polymer material and interfacial seepage at the boundary may take place simultaneously, resulting in concurrent existence of both seepage modes.

An analysis of the critical condition for the failure of a single spherical foam cell within the polymer material subjected to hydraulic flow was performed (see Fig. 12). A simplified assumption was made that the foam cell geometry is perfectly spherical in shape. It is postulated that failure of the cell wall occurs when the applied water pressure

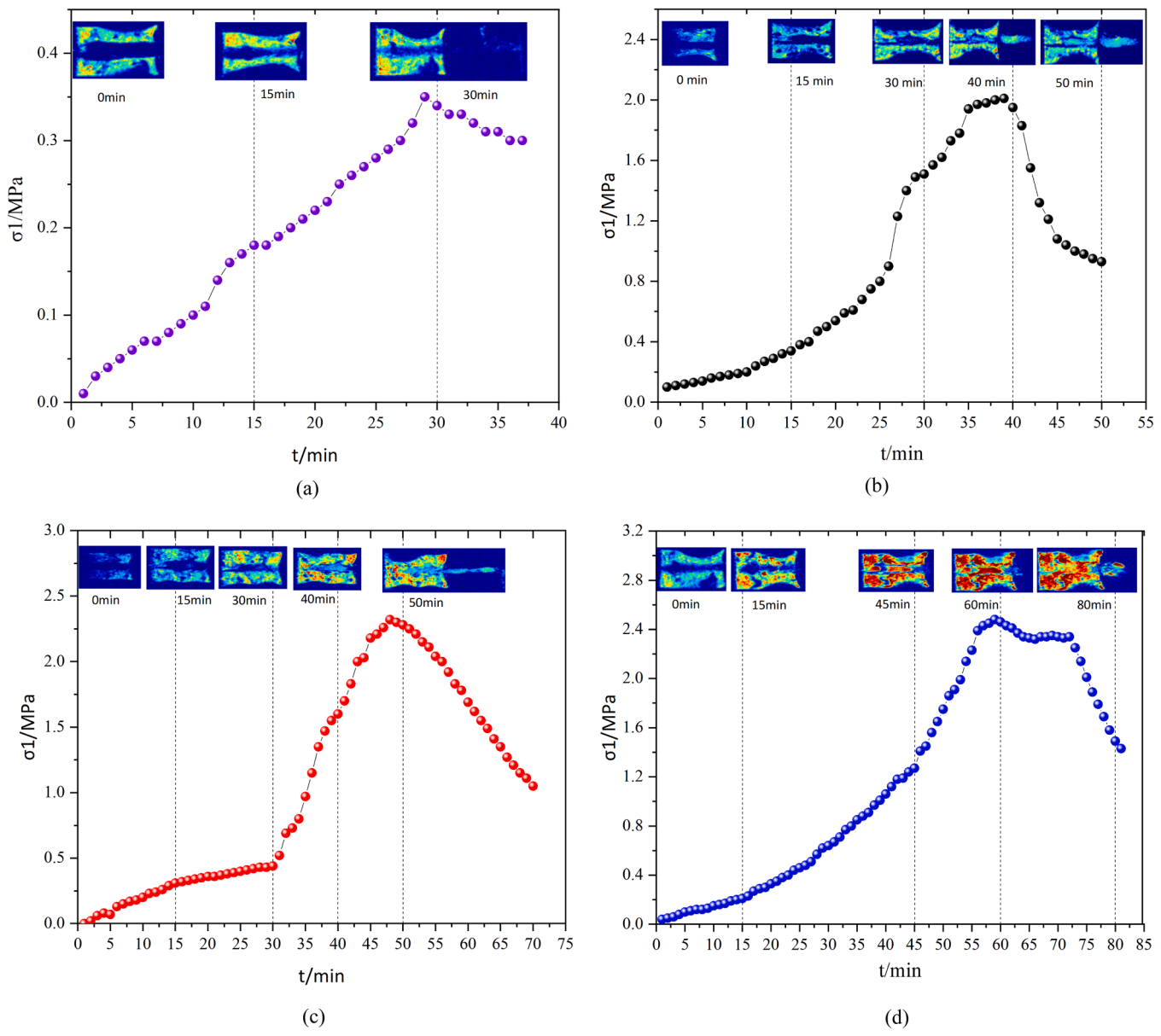

Fig. 11. Changes in the inlet pressure during water flooding for the grouting body with different grouting mass: (a) 7 g, (b) 10 g, (c) 15 g and (d) 20 g.

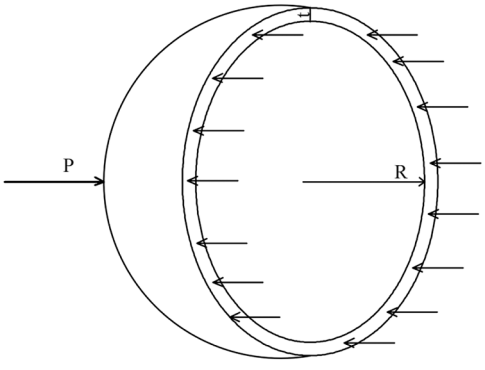

Fig. 12. Schematic diagram of stress exerted on a polymer foam cell under seepage water pressure.

on the wall exceeds the compressive strength of the cell wall material. The critical pressure condition for foam cell failure can thus be mathematically expressed as

$$P \times \pi R^2 = \sigma_c \times 2\pi Rt \tag{7}$$

where P denotes the water pressure exerted on the cell wall, t represents the cell wall thickness, $R$is the radius of the spherical foam cell and $\sigma_c$is the compressive strength of the cell wall material.

The critical rupture pressure for the foam cell can be obtained as

$$P_c = \sigma_c \times t/R \tag{8}$$

The above formula indicates that the critical rupture pressure of the foam cell is inversely proportional to the cell radius and directly proportional to the wall thickness and compressive strength of the cell wall. As the density of the polymer increases, the foam cell radius decreases while the wall thickness and compressive strength increase. Therefore, the overall ability of the polymer foam cells to resist external pressure-induced rupture mainly depends on the material density. Based on this, in the practical design of grouting and leakage plugging engineering, the

polymer slurry formula with an appropriate density can be selected according to the hydraulic head pressure magnitude of the permeation fluid at the target burial site, in order to meet the specific application requirements for resisting seepage rupture.

5.2. Influence of polymer density on the anti-seepage effect of grouting body

Fig. 13 shows the relationship curves between the density of the grouting body and the seepage initiation pressure as well as the seepage duration. As the density of the polymer increased, the seepage initiation pressure of the grouting body exhibited an ascending trend. The seepage duration underwent substantial prolongation.

When the polymer density was relatively low (e.g. 0.23 g/cm^3), due to insufficient expansion force of the polymer, it cannot provide adequate shear resistance at the interface. Under the action of water flow, slipping and cracking easily occurred at the polymer-geomembrane interface, resulting in seepage along the interface. In this case, the low density polymer grouting body had weaker resistance against water pressure, and interfacial seepage also occurred within a shorter period. In engineering practice, excessively low grouting mass and polymer density should be avoided, which can lead to inadequate interfacial shear strength. Alternatively, other measures can be taken to enhance the interfacial shear strength between polymer and geomembrane, in order to prevent such interfacial slippage, cracking and seepage failures. In contrast, when the polymer density was relatively high (e.g., 0.33 g/cm^3 or above), the interfacial shear strength between polymer and geomembrane was greater, and the seepage water tended to leak from weaker areas inside the polymer. Since the polymer had a discontiguous closed-cell structure, the water flow relied on gradually penetrating the foam cells inside the matrix to form seepage channels, which took more time and required higher water pressures (e.g. above 2 MPa) to break through. Under such circumstances, the high-density grouting body can withstand greater water pressures. Its impermeability was significantly improved, delaying the occurrence of seepage.

Therefore, the polymer density is a critical parameter determining the impermeability of the grouting mixture and is positively correlated with the ability of the grouting mixture to resist water pressure.

6. Conclusions

Utilizing nuclear magnetic resonance techniques, this study monitored the seepage process through the polymer grouting body with varying densities. The anti-seepage performance and mechanism of seepage failure was investigated. The key conclusions are summarized as follows:

(1) Under the action of water flow, two archetypal seepage failure mechanisms of the polymer grouting body were discerned. Firstly, interfacial seepage occurred due to deficient expansive force of the polymer, leading to conferring inferior interfacial shear strength. Secondly, internal seepage within the polymer matrix occurred when the exerted pressure exceeded the intrinsic compressive strength threshold of the foam cells, resulting in deformational failure.

(2) Avoiding interfacial seepage can significantly improve the impermeability of the grouting body. The findings of this study reveal that with an 8 mm-diameter hole in the geomembrane and a polymer density of 0.23 g/cm^3, seepage occurred predominantly at the polymer-geomembrane interface, with an associated inception pressure of approximately 0.35 MPa. However, when the polymer density was increased to 0.33 g/cm^3 and above, the seepage occurred principally within the polymer, with a corresponding inception pressure surpassing 2 MPa.

(3) The compressive strength of the polymer foam cells was positively correlated with the polymer density. As the density of the polymer increased, a reduction in the average diameter of the foam cells was observed, alongside thickening of the cell walls. This induced superior compressive strength of the foamed cells, conferring an improved capacity to withstand external compressive deformation.

(4) The polymer density is a key parameter determining the anti-seepage performance of the grouting body, exhibiting a positive correlation with the capacity to withstand hydraulic pressure. Elevating the polymer density enhanced both the interfacial shear resistance and compressive strength of the foam cells, thereby comprehensively augmenting the waterproofing capabilities of the grouting body.

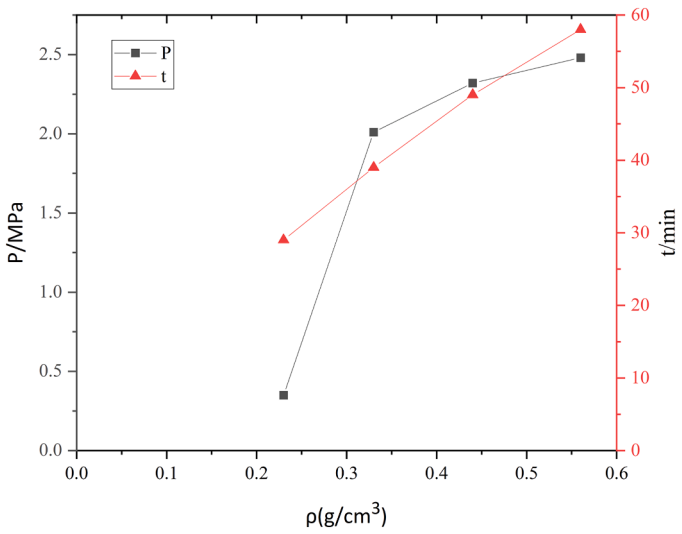

Fig. 13. Variations in seepage initiation pressure and seepage duration of the grouting body with different polymer densities.

Overall, the polymer grouting technique has the potential to effectively repair the defects of geomembranes in landfill. However, during practical implementation, various challenges are encountered. To assess the long-term performance of the polymer grouting body, it is necessary to conduct model tests and field tests under various conditions that may involve chemical corrosion, thermal aging, and mechanical effects.

CRediT authorship contribution statement

Zhai Kejie: Conceptualization. **Wang Fuming:** Writing – review & editing, Supervision, Conceptualization. **Chu Xuanxuan:** Writing – review & editing. **Ke Qiuju:** Writing – original draft, Formal analysis, Data curation, Conceptualization. **Guo Chengchao:** Writing – review & editing, Conceptualization.

Declaration of Competing Interest

The authors declare that they have no known competing financial interests or personal relationships that could have appeared to influence the work reported in this paper.

Data availability

No data was used for the research described in the article.

Acknowledgments

This research was supported by the National Key Research and Development Program of China (Grant No. 2021YFC3100800, 2021YFC3100803).

References

[1] R.K. Rowe, M.Z. Islam, R.W.I. Brachman, et al., Antioxidant depletion from a high density polyethylene geomembrane under simulated landfill conditions[J], J. Geotech. Geoenviron. Eng. 136 (7) (2010) 930–939, https://doi.org/10.1061/(ASCE)GT.1943-5606.0000302.

[2] R.K. Rowe, S. Rimal, H. Sangam, Ageing of HDPE geomembrane exposed to air, water and leachate at different temperatures[J], Geotext. Geomembr. 27 (2) (2009) 137–151, https://doi.org/10.1016/j.geotexmem.2008.09.007.

[3] C.C. White, R. D, et al., Electrical leak detection system for landfill liners: a case history[J], Ground Water Monit. Remediat. 17 (3) (1997) 153–159, https://doi.org/10.1111/j.1745-6592.1997.tb00590.x.

[4] Q. Ke, C. Guo, H. Ma, et al., Laboratory study on corrosion resistance of polyurethane grouting material in landfill site[J], Environ. Geotech. (2022), https://doi.org/10.1680/jenge.22.00020.

[5] R.K. Rowe, Protecting the environment with geosynthetics: 53rd Karl Terzaghi Lecture[J], J. Geotech. Geoenviron. Eng. 146 (9) (2020), https://doi.org/10.1061/(ASCE)GT.1943-5606.0002239.

[6] Rumer R., Mitchell J. Assessment of barrier containment technologies: a comprehensive treatment for environmental reemedi[M]. Assessment of barrier containment technologies: a comprehensive treatment for environmental reemedi, 1995.

[7] Gregory, P. Van, et al., Monitoring leaks from storage ponds using resistivity methods[J], Geophysics (1991), https://doi.org/10.1190/1.1443147.

[8] R. Drochytka, J. Hodul, L. Mészárosová, et al., Chemically resistant polymeric jointing grout with environmental impact[J], Constr. Build. Mater. 292 (11) (2021) 123454, https://doi.org/10.1016/j.conbuildmat.2021.123454.

[9] B. Sun, C. Guo, Y. Chen, et al., Study on spraying construction method of a non-water reacting polymer layer in the tunnel[J], Materials 15 (12) (2022) 4138, https://doi.org/10.3390/ma15124138.

[10] L. Qin, C. Guo, W. Sun, et al., Experimental study on interfacial damage characteristics of CRTS II slab track and CA mortar with AE and DIC techniques[J], Eng. Fail. Anal. 142 (2022) 106777, https://doi.org/10.1016/j.engfailanal.2022.106777.

[11] H. Fang, B. Li, F. Wang, et al., The mechanical behaviour of drainage pipeline under traffic load before and after polymer grouting trenchless repairing[J], Tunn. Undergr. Space Technol. Inc. Trench Technol. Res. 74 (2018) 185–194, https://doi.org/10.1016/j.tust.2018.01.018.

[12] G. Chengchao, W. Fuming, Mechanism study on the construction of ultra-thin antiseepage wall by polymer injection[J], J. Mater. Civ. Eng. 24 (9) (2012) 1183–1192, https://doi.org/10.1061/(ASCE)MT.1943-5533.0000497.

[13] X. Li, T. Zhang, M. Hao, et al., Unsplit Youngs method for tracking the moving interface of expansible grout[J], Complexity 2020 (2020) 1–17, https://doi.org/10.1155/2020/2014959.

[14] Y. Wang, M. Han, B. Li, et al., Stability evaluation of earth-rock dam reinforcement with new permeable polymer based on reliability method[J], Constr. Build. Mater. 320 (2022) 126294, https://doi.org/10.1016/j.conbuildmat.2021.126294.

[15] C. Guo, B. Sun, D. Hu, et al., A field experimental study on the diffusion behavior of expanding polymer grouting material in soil[J], Soil Mech. Found. Eng. 56 (3) (2019) 171–177, https://doi.org/10.1007/s11204-019-09586-7.

[16] R. Wang, F. Wang, J. Xu, et al., Full-scale experimental study of the dynamic performance of buried drainage pipes under polymer grouting trenchless rehabilitation[J], Ocean Eng. 181 (2019) 121–133, https://doi.org/10.1016/j.oceaneng.2019.04.009.

[17] M. Hao, X. Li, Y. Zhong, et al., Experimental study of polyurethane grout diffusion in a water-bearing fracture[J], J. Mater. Civ. Eng. 33 (3) (2021), https://doi.org/10.1061/(ASCE)MT.1943-5533.0003612.

[18] X. Du, H. Fang, K. Liu, et al., Experimental and practical investigation of reinforcement mechanism on permeable polymer in loose area of drainage pipeline [J], Tunn. Undergr. Space Technol. 140 (2023) 105250, https://doi.org/10.1016/j.tust.2023.105250.

[19] Z. Zhou, X. Du, S. Wang, et al., Micromechanism of the diffusion of cement-based grouts in porous media under two hydraulic operating conditions: constant flow rate and constant pressure[J], ACTA GEOTECHNICA 14 (3) (2019) 825–841, https://doi.org/10.1007/s11440-018-0704-z.

[20] Z. Sun, J. Zhang, Y. Sun, Feasibility of a polymer foaming agent as a grouting material for broken coal masses[J], Adv. Civ. Eng. 2019 (2019) 1–9, https://doi.org/10.1155/2019/9084861.

[21] V. Loskutov, S. Zhakov, Dependence of the liquid transverse relaxation time T2 in porous media on fluid flow velocity[J], Int. J. Heat. Mass Transf. 101 (2016) 692–698, https://doi.org/10.1016/j.ijheatmasstransfer.2016.05.057.

[22] Y.L. Xu, X.L. Li, X.K. Wu, et al., Experimental study on pore fluid characteristics of fractured sandstone based on nuclear magnetic resonance technology[J], J. Pet. Sci. Eng. 214 (2022), https://doi.org/10.1016/j.petrol.2022.110408.

[23] M. Tang, T. Zhang, Y. Ma, et al., Experimental study on fracture effect on the multiphase flow in ultra-low permeability sandstone based on LF NMR[J], Geoenergy Sci. Eng. 222 (2023), https://doi.org/10.1016/j.geoen.2022.211399.

[24] L. Weng, Z. Wu, S. Zhang, et al., Real-time characterization of the grouting diffusion process in fractured sandstone based on the low-field nuclear magnetic resonance technique[J], Int. J. Rock. Mech. Min. Sci. 152 (2022), https://doi.org/10.1016/j.ijrmms.2022.105060.

[25] B. Wei, X. Zhang, R. Wu, et al., Pore-scale monitoring of CO_2 and N_2 flooding processes in a tight formation under reservoir conditions using nuclear magnetic resonance (NMR): a case study[J], FUEL 246 (2019) 34–41, https://doi.org/10.1016/j.fuel.2019.02.103.

[26] T. Zhang, M. Tang, Y. Ma, et al., Experimental study on CO_2/water flooding mechanism and oil recovery in ultralow - permeability sandstone with online LF NMR[J], ENERGY 252 (2022), https://doi.org/10.1016/j.energy.2022.123948.